THE PUBLISHING HOUSE
OF THE ROMANIAN ACADEMY

PROCEEDINGS OF THE ROMANIAN ACADEMY, Series A,
Volume 15, Number 3/2014, pp. 272–282

THE ELECTROMECHANICAL IMPEDANCE METHOD FOR STRUCTURAL HEALTH MONITORING OF THIN CIRCULAR PLATES

Cristian RUGINA[1], Adrian TOADER [2], Victor GIURGIUTIU [2,3], Ioan URSU [2]

[1] Institute of Solid Mechanics of the Romanian Academy
[2] "Elie Carafoli" National Institute for Aerospace Research (INCAS)
[3] University of South Carolina, Columbia, SC 29208, USA
e-mail: rugina.cristian@gmail.com

This paper describes the electro-mechanical (E/M) impedance method applied to structural health monitoring (SHM) of thin circular plates. The method allows us to identify the local dynamics of the structure directly through the E/M impedance signatures of piezoelectric wafer active sensors (PWAS) permanently mounted to the structure. An analytical model for 2-D thin-wall structures, which predicts the E/M impedance response at PWAS terminals, was developed and validated. The model accounts for axial and flexural vibrations of the structure and considers both the structural dynamics and the sensor dynamics. Calibration experiments performed on circular thin plates with centrally attached PWAS show that the presence of a damage modifies the high-frequency E/M impedance spectrum causing frequency shifts, peak splitting, and appearance of new harmonics. Comparisons between the analytical method, the finite element method, and experiments were performed, with a fabricated structural arc-shape defect.

Key words: structural health monitoring, electro-mechanical impedance method, piezoelectric wafer active sensors, circular thin plate.

1. INTRODUCTION

The active SHM sensing techniques are based on two different approaches: transient guided waves and standing waves [1, 2]. In such SHM processes, a PWAS is required to generate elastic waves. These travel along the mechanical structure, are reflected by different structural abnormalities, or boundary edges, and then are recaptured by the same sensor in a pulse-echo configuration or by other sensors of same or different type, even passive sensors, in pitch-catch configuration [1]. If the structural damage or boundary edges are in the close vicinity of the active sensor, their reflections overlap the incident transient wave, making impossible the interpretation. This drawback can be overpassed by using the ultrasonic standing waves, in the so-called electromechanical impedance (E/M) method [1, 2]; by sweeping the frequency of the input signals to PWAS, some changes appear in the impedance, measured by an impedance analyzer connected to the PWAS terminals. By monitoring the changes in the real part of the impedance function, which is most sensitive to structural changes, one can evaluate the integrity of the host structure.

It is worthy of note that the SHM, vibration and fatigue control, flutter suppression, gust load alleviation, maneuvers load alleviation and optimization of adaptive wing structures, all together compose an inventory of technologies, attentively evaluated in the framework of the ambitious EU project CleanSky SFWA (CleanSky – Smart Fixed Wing Aircraft, Integrated Technology Demonstrator – ITD, Seventh Framework Programme, see http://www.cleansky.eu), having INCAS Cluster as Associate Partner (see http://www.incas.ro and [3, 4]).

This paper describes a unitary and self-contained mathematical modeling and analytical solution for the E/M impedance of a circular aluminum plate, PWAS instrumented. This approach serves as a reference point for extending the method to other models with unusual geometries. Further, are presented, for comparison, the simulation of the analytical solution, followed by numerical solution based on finite element method. Finally, the two solutions, analytical and numerical, are compared with experimental results, measured on aluminum disks, with and without a laser fabricated defect.

2. ANALYTICAL SOLUTION OF E/M IMPEDANCE FOR A CIRCULAR PLATE

The classical differential equation of motion for the transverse displacement w of a plate is [5]:

$$D\nabla^4 w + \rho h \frac{\partial^2 w}{\partial t^2} = 0,\ D = \frac{Eh^3}{12\left(1-\nu^2\right)}, \tag{1}$$

where: D is the transverse (flexural) rigidity, E is Young's modulus, h is the plate thickness, ν is Poisson's ratio, ρ is mass density per unit area of the plate, t is time, and $\nabla^4 = \nabla^2\nabla^2$, where ∇^2 is the Laplace operator.

2.1. General solution for flexural vibration of a circular plate

The study of the flexural vibration of circular plates has a rich history comprising works and classical studies, e.g., [6]. Some of the main results in the field will be inventoried in the following. Assuming time harmonic vibrations and taking polar coordinates (r, θ), the space and time dependencies will be considered as separated and thus the displacement is expressed in the form:

$$w(r,\theta,t) = \hat{w}(r,\theta)\mathrm{e}^{\mathrm{i}\omega t}. \tag{2}$$

The problem is to find the space-dependent solution $\hat{w}(r,\theta)$ such that it satisfies the differential equation (1) and certain boundary conditions. Equation (1) becomes, after factorization:

$$\left(\nabla^2+\gamma^2\right)\left(\nabla^2-\gamma^2\right)\hat{w} = 0,\ \gamma^4 = \frac{\rho h}{D}\omega^2,\ \nabla^2 = \frac{\partial^2}{\partial r^2} + \frac{1}{r}\frac{\partial}{\partial r} + \frac{1}{r^2}\frac{\partial^2}{\partial\theta^2}. \tag{3}$$

The complete solution to equation (3) is obtained by superposition of the solutions of the system:

$$\left(\nabla^2+\gamma^2\right)\hat{w}_1 = 0,\ \left(\nabla^2-\gamma^2\right)\hat{w}_2 = 0. \tag{4}$$

The solution of equation (1) is searched in the general Fourier form:

$$\hat{w}(r,\theta) = \sum_{n=0}^{\infty} W_n(r)\cos n\theta + \sum_{n=0}^{\infty} W_n^*(r)\sin n\theta. \tag{5}$$

The substitution of equation (5) into equations (4) gives:

$$\frac{\mathrm{d}^2 W_{1_n}}{\mathrm{d}r^2} + \frac{1}{r}\frac{\mathrm{d}W_{1_n}}{\mathrm{d}r} - \left(\frac{n^2}{r^2}-\gamma^2\right)W_{1_n} = 0,\ \frac{\mathrm{d}^2 W_{2_n}}{\mathrm{d}r^2} + \frac{1}{r}\frac{\mathrm{d}W_{2_n}}{\mathrm{d}r} - \left(\frac{n^2}{r^2}+\gamma^2\right)W_{2_n} = 0, \tag{6}$$

and two other similar equations for W_n^*. Equations (6) are Bessel equations [7] having solutions:

$$W_{1_n} = A_n J_n(\gamma r) + B_n Y_n(\gamma r),\ W_{2_n} = F_n I_n(\gamma r) + G_n K_n(\gamma r), \tag{7}$$

where J_n and Y_n are the Bessel functions of the first and second kind and order n, whereas I_n and K_n are the modified Bessel functions of the first and second kind and order n [7]. The coefficients A_n, B_n, C_n, D_n are found by the imposition of the boundary and initial conditions. The general solution of equation (3) is:

$$\begin{aligned}\hat{w}(r,\theta) = &\sum_{n=0}^{\infty}\left[A_n J_n(\gamma r) + B_n Y_n(\gamma r) + F_n I_n(\gamma r) + G_n K_n(\gamma r)\right]\cos n\theta + \\ &+\sum_{n=0}^{\infty}\left[A_n^* J_n(\gamma r) + B_n^* Y_n(\gamma r) + F_n^* I_n(\gamma r) + G_n^* K_n(\gamma r)\right]\sin n\theta.\end{aligned} \tag{8}$$

However, the Bessel functions $Y_n(\gamma r)$ and $K_n(\gamma r)$ have infinite values at $r=0$ and are discarded (unless the plate has a hole around $r=0$, which is not the case considered here). This means, for solid plates without a central hole, the terms of equation (8) involving $Y_n(\gamma r)$ and $K_n(\gamma r)$ are discarded because they become unbounded at $r=0$. In addition, if the boundary conditions have some symmetry with respect to at least one diameter, then the terms in $\sin n\theta$ are not needed. Where these assumptions are employed, equation (8) simplifies to [5] ($n=0,1,\ldots$ represents the number of nodal diameters):

$$W_n=\left[A_nJ_n(\gamma r)+F_nI_n(\gamma r)\right]\cos n\theta\,. \tag{9}$$

2. 2. Flexural vibration of free circular plates

Consider the volume $\mathrm{d}V=h\,r\,\mathrm{d}r\,\mathrm{d}\theta$ of a differential element in cylindrical coordinates. Bending and twisting moments $M_r, M_\theta, M_{r\theta}, M_{\theta r}$ are related to the flexural displacement w by [5]:

$$\begin{gathered}M_r=-D\left[\frac{\partial^2 w}{\partial r^2}+\nu\left(\frac{1}{r}\frac{\partial w}{\partial r}+\frac{1}{r^2}\frac{\partial^2 w}{\partial\theta^2}\right)\right],\ M_\theta=-D\left[\frac{1}{r}\frac{\partial w}{\partial r}+\frac{1}{r^2}\frac{\partial^2 w}{\partial\theta^2}+\nu\frac{\partial^2 w}{\partial r^2}\right],\\ M_{r\theta}=M_{\theta r}=-(1-\nu)D\left[\frac{1}{r}\frac{\partial^2 w}{\partial r\partial\theta}-\frac{1}{r^2}\frac{\partial w}{\partial\theta}\right].\end{gathered} \tag{10}$$

Transverse shearing forces Q_r, Q_θ are related to the flexural displacement, w, in the form:

$$Q_r=-D\frac{\partial}{\partial r}\left(\nabla^2 w\right),\ Q_\theta=-D\frac{1}{r}\frac{\partial}{\partial\theta}\left(\nabla^2 w\right). \tag{11}$$

The Kelvin-Kirchhoff edge reactions in polar coordinates are given by:

$$V_r=Q_r+\frac{1}{r}\frac{\partial M_{r\theta}}{\partial\theta},\ V_\theta=Q_\theta+\frac{\partial M_{r\theta}}{\partial r}. \tag{12}$$

The boundary conditions for a free circular plate of outer radius a are:

$$M_r(a)=0,\ V_r(a)=0. \tag{13}$$

The substitution of boundary conditions (13) into equations (10), (12), with the use of Eq. (11) yields the characteristic equation [7, p. 10]:

$$\frac{\lambda^2J_n(\lambda)+(1-\nu)\left[\lambda J_n'(\lambda)-n^2J_n(\lambda)\right]}{\lambda^2I_n(\lambda)-(1-\nu)\left[\lambda I_n'(\lambda)-n^2I_n(\lambda)\right]}=\frac{\lambda^3J_n'(\lambda)+(1-\nu)n^2\left[\lambda J_n'(\lambda)-J_n(\lambda)\right]}{\lambda^3I_n'(\lambda)-(1-\nu)n^2\left[\lambda I'(\lambda)-I_n(\lambda)\right]}, \tag{14}$$

where $\lambda=\gamma a$. Itao and Crandall [8] performed a comprehensive numerical solution of eigenvalue roots of the characteristic equation (14) and of the associated mode shapes. The eigenvalues of equation (14) were presented as $\lambda_{j,p}$, where $j=1,2,\ldots$ is the number of *nodal circles* and $p=0,1,\ldots$ is the number of *nodal diameters*. (The case $j=0$ yields a triple root at $\lambda=0$ that corresponds to three rigid-body motion modes of a free plate). The mode shapes were presented in the form:

$$W_{j,p}(r,\theta)=A_{j,p}\left[J_p(\lambda_{j,p}r/a)+C_{j,p}I_p(\lambda_{j,p}r/a)\right]\cos p\theta\,. \tag{15}$$

A sample of values for the eigenvalue $\lambda_{j,p}$, the mode shape parameter $C_{j,p}$, and amplitude $A_{j,p}$ are given in Itao and Crandall [8]. The mode shapes amplitudes $A_{j,p}$ [10] were found based on the mass-normalization formula and mode shapes orthogonality (m is the total mass of the plate and δ_{ij} is the Kronecker delta):

$$\int_0^{2\pi}\int_0^a \rho\, h\, W_{j,p}^2(r,\theta)\, r\mathrm{d}r\mathrm{d}\theta = \rho\pi a^2 h = m,\ \int_0^{2\pi}\int_0^a \rho h W_{j,p} W_{i,q}\, r\mathrm{d}r\mathrm{d}\theta = m\delta_{ij}\delta_{pq}\,. \tag{16}$$

2. 3. Circular plates: particular case of axisymmetric free flexural vibration

Axisymmetric flexural vibration of a circular plate can be understood in terms of standing circular-crested waves that propagate in a concentric circular pattern from the center of the plate and reflect at the plate circumference. The problem is θ-invariant, i.e. $\partial/\partial\theta = 0$. The general solution (2) is sought in the form:

$$w(r,t) = \hat{w}(r)\mathrm{e}^{\mathrm{i}\omega t}\,. \tag{17}$$

By substitution in equation (1), the decomposition (3) is retrieved:

$$\left(\frac{\mathrm{d}^2}{\mathrm{d}r^2} + \frac{1}{r}\frac{\mathrm{d}}{\mathrm{d}r} + \gamma^2\right)\hat{w} = 0 \quad \text{or} \quad \left(\frac{\mathrm{d}^2}{\mathrm{d}r^2} + \frac{1}{r}\frac{\mathrm{d}}{\mathrm{d}r} - \gamma^2\right)\hat{w} = 0\,. \tag{18}$$

Fourier form (5) is no longer present, given the absence of $\theta-$dependence. This is equivalent to $n = 0$ in the equations (8) and thus the general solution for axisymmetric flexural vibration of circular plates has the form

$$w(r,t) = \left[AJ_0(\gamma r) + FI_0(\gamma r)\right]e^{i\omega t}\,, \tag{19}$$

where $J_0(\gamma r)$ is the Bessel function of first kind and order zero, whereas $I_0(\gamma r)$ is the modified Bessel function of first kind and order zero. The constants are to be determined from the initial and boundary conditions. From the same reasons shown in Section 2.1, the functions $Y_0(\gamma r)$ and $K_0(\gamma r)$ were discarded. Closely following equations (10)-(14), one gets the characteristic transcendental equation:

$$\frac{\lambda^2 J_0(\lambda) + (1-\nu)\lambda J_0'(\lambda)}{\lambda^2 I_0(\lambda) - (1-\nu)\lambda I_0'(\lambda)} = \frac{\lambda^3 J_0'(\lambda)}{\lambda^3 I_0'(\lambda)},\quad \lambda = \gamma a,\quad \omega_j = \lambda_j^2\sqrt{\frac{D}{\rho h a^4}}\,. \tag{20}$$

That gives natural frequencies ω_j associated with each eigenvalue λ_j and mode shape. For each eigenvalue, one finds the corresponding mode shape by calculating the constants A and F in the equation (19). The general expression of the mode shape is written using an amplitude A_j and a mode shape parameter C_j, i.e.,

$$W_j(r) = A_j\left[J_0(\lambda_j r/a) + C_j I_0(\lambda_j r/a)\right]. \tag{21}$$

From the normalization relationships (16), one obtains [10]:

$$A_j = \frac{1}{\sqrt{2}}\left\{\left[J_0(\lambda_j) + C_j I_0(\lambda_j)\right]^2 - \left[J_0'(\lambda_j)\right]^2 - \left[C_j I_0'(\lambda_j)\right]^2\right\}^{-\frac{1}{2}}. \tag{22}$$

2.4. Forced axisymmetric flexural vibration of circular plates

Consider the circular plate undergoing axisymmetric flexural vibration under the excitation of an externally applied time-dependent distributed moment $m_e(r,t)$ (Fig. 2.1, left). The units of $m_e(r,t)$ are moment per unit area (e. g., Nm/ m^2). Let ω_j, $W_j(r)$ and A_j described by (20), (21), and (22), respectively.

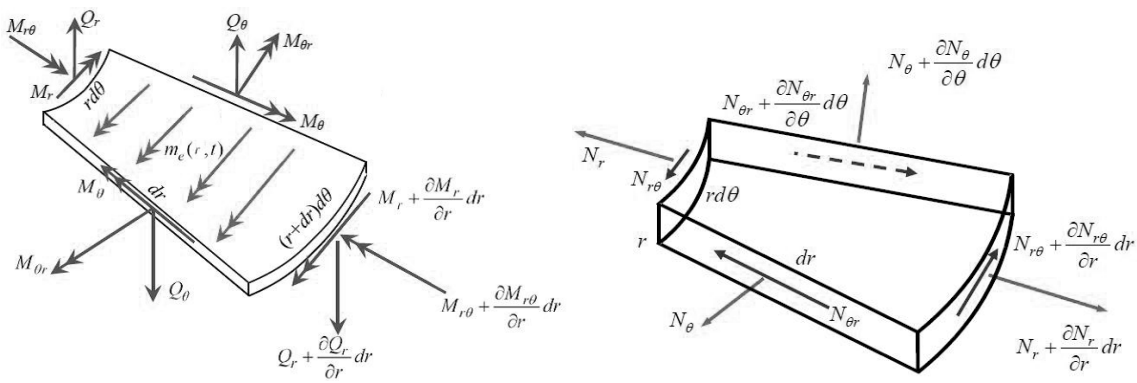

Fig. 2.1 – Circular plate. Left: sketch for flexural vibration analysis; right: sketch for axial vibration analysis.

PROPOSITION 2.1. *The equation of motion for forced vibrations of the circular plate under axisymmetric flexural moment excitation and its solution are:*

$$D\nabla^4 w + \rho h\ddot{w} = \hat{m}_e' + \hat{m}_e / r\,. \tag{23}$$

$$\begin{aligned} w(r,t) &= \frac{2}{\rho\, ha^2}\sum_{j=1}^{\infty}\frac{f_j}{-\omega^2 + +2i\,\zeta_j\,\omega\omega_j + \omega_j^2}W_j(r)\,\mathrm{e}^{\mathrm{i}\omega t}, \\ f_j &= a\,\hat{m}_e(a)W_j(a) - \int_0^a \hat{m}_e(r)W_j'(r)\,r\mathrm{d}r,\ j = 1, 2, 3, \ldots \end{aligned} \tag{24}$$

Proof. For reasons of space, we only sketch the proof. Apply free-body analysis in the *r*-direction to an infinitesimal plate element $r\,\mathrm{d}r\,\mathrm{d}\theta$. Equations for force and moments are obtained in the form $Q_r + r(\partial Q_r/\partial r) = \rho hr\,\ddot{w}$, $r(\partial^2 M_r/\partial r^2) + 2(\partial M_r/\partial r) - (\partial M_\theta/\partial r) + m_e + r(\partial m_e/\partial r) = \rho hr\,\ddot{w}$; substituting of those in (10) gives (23), and assuming both excitation and response are harmonic, we have:

$$m_e(r,t) = \hat{m}_e(r)\,\mathrm{e}^{\mathrm{i}\omega t},\ w(r,t) = \sum_{j=1}^{\infty}\eta_j W_j(r)\,\mathrm{e}^{\mathrm{i}\omega t}\ . \tag{25}$$

The constants η_j are the modal participation factors. Substitution of Eq. (25) into equation (23), division by $\mathrm{e}^{\mathrm{i}\omega t}$, use of natural frequencies ω_i described by the equation $D\nabla^4 W_i - \omega^2\rho_i hW_i = 0$, recalling (16) and deliberate introduction of modal damping ζ_j lead to expressions (24), so completing the proof.

2.5. General solution for the axisymmetric axial vibration of circular plates

Consider the infinitesimal plate element in polar coordinates shown in Fig. 2.1 right. Under the axisymmetric assumption, the wave equation in polar coordinates is:

$$c_L^2\nabla^2 u_r - \ddot{u}_r = 0,\ c_L^2 = E/\left(\rho(1-\nu^2)\right), \tag{26}$$

where c_L is the longitudinal wave speed in plate. Stress-displacement relations of elasticity theory were used, followed by integration of stresses across the thickness and the free-body analysis applied to element Similarly to the approach at the beginning of paragraph 2.1, the displacement u_r is considered harmonic:

$$u_r(r,t) = \hat{u}(r)\,\mathrm{e}^{\mathrm{i}\omega t}\,. \tag{27}$$

Substitution in (26) yields a Bessel equation. Introducing the wavenumber γ, the same considerations as those at the end of paragraph 2.1 lead to the solution:

$$u_r(r,t) = AJ_1(\gamma r)\mathrm{e}^{\mathrm{i}\omega t},\ \gamma = \omega/c_L\ . \tag{28}$$

The constant A, the frequency ω, and the wavenumber γ are determined from the boundary condition $N_r(a)=0$, which means $\left.\left(\frac{\partial u_r}{\partial r}+\nu\frac{u_r}{r}\right)\right|_{r=a}=0$. Substituting (27) in the last equation and applying standard reasoning, we obtain the characteristic equation, the constant A_n and the mode shapes U_n :

$$zJ_0(z)-(1-\nu)J_1(z)=0,\ A_n=\left(J_1^2(z_n)-J_0(z_n)J_2(z_n)\right)^{-0.5},\ \omega_n=c_L(\gamma a)_n/a,\ U_n(r)=A_nJ_1(\gamma_n r), \tag{29}$$

where $z=\gamma a$, $\gamma_n=c_L(\gamma a)_n/a=z_n/a$. Mode shapes U_n are orthonormal, $\int_0^a U_p(r)U_q(r)r\mathrm{d}r=a^2\delta_{pq}/2$, with respect to weight function r (as for flexural vibrations). Indeed, the afferent Bessel equation is related to a Sturm-Liouville problem: $(rU')'+\left(\gamma^2 r-r^{-1}\right)U=0$, $U_i'(a)+U_i(a)=0,\ i=p,q.$

2.6. Forced axisymmetric axial vibration of circular plates

Consider the circular plate undergoing axisymmetric axial vibration under the excitation of an externally applied time-dependent distributed axial force $f(r,t)$ (Fig. 2.1, left). The units of $f(r,t)$ are force per unit area (e. g., Nm/ m^2). Consider $U_j(r)$, ω_j described by (29).

PROPOSITION 2.2. *The equation of motion for forced axial vibrations of the circular plates under axisymmetric axial force excitation and its solution are, respectively:*

$$c_L^2\nabla^2 u_r-\ddot{u}_r=-\frac{f}{\rho h},u_r(r,t)=\frac{2}{\rho ha^2}\sum_{j=1}^{\infty}\frac{f_j\,U_j(r)\mathrm{e}^{\mathrm{i}\omega t}}{-\omega^2+2i\zeta_j\,\omega\omega_j+\omega_j^2},\quad f_j=\int_0^a\hat{f}(r)U_j(r)r\mathrm{d}r,\ j=1,2,3,.. \tag{30}$$

Proof. A simple application of the free-body analysis in the r-direction to an infinitesimal plate element $r\,\mathrm{d}r\mathrm{d}\theta$ gives the first equation in (30). Further, it is assumed that excitation and response are harmonic $f(r,t)=\hat{f}(r)\mathrm{e}^{\mathrm{i}\omega t}$, $u_r(r,t)=u_r(r)\mathrm{e}^{\mathrm{i}\omega t}$. The substitution of the modal form $\hat{u}(r)=\sum_j U_j(r)\eta_j$, ($\eta_j$ are modal participation factors) in the equation of motion, the use of natural frequencies ω_i and the deliberate introduction of modal damping ζ_j lead to the other two expressions (30).

2.7. The interaction between a circular PWAS and a circular plate. Electromechanical impedance

The E/M method is exemplified in the case of a 2-D PWAS circular modal sensor bonded on a thin isotropic circular plate (Fig. 2.2). The basic concept of the method is to use high frequency structural excitations to monitor the local area of a structure for changes in structural impedance that would indicate imminent damage. This is possible using PWAS sensor/actuators whose electrical impedance is directly related to the structure mechanical impedance. The structural dynamics affects the PWAS response; it modifies the PWAS E/M impedance, measured by an impedance analyzer connected to the PWAS terminals.

It is assumed that the circumferential boundary of the PWAS disc is conditioned by the structure through the dynamic stiffness $k_{str}(\omega)$, which includes both axial and flexural vibration modes. The problem is formulated in terms of interaction line force, F_{PWAS}, and the corresponding displacement, u_{PWAS}, measured at the PWAS circumference. The units of F_{PWAS} are force per unit length (e.g., N/m). The corresponding distributed excitation axial force and flexural moment are expressed as, respectively:

$$f_e(r,t)=\hat{f}_e(r)\mathrm{e}^{\mathrm{i}\omega t}=\hat{F}_{PWAS}\mathrm{e}^{\mathrm{i}\omega t}\delta(r-r_a)/r,\ m_e(r,t)=m_e(r)\mathrm{e}^{\mathrm{i}\omega t}=h\hat{F}_{PWAS}\delta(r-r_a)/(2r). \tag{31}$$

By dividing the Dirac function δ with r, its total effect around a circular circumference does not change when radius changes. Consider ω_{j_u}, $U_{j_u}(r_a)$, ω_{j_w}, $W_{j_w}(r_a)$, described by (29), (20), (21), respectively.

PROPOSITION 2.3. *The dynamic structural stiffness* $k_{str}(\omega)$ *constraining PWAS sensor is given by:*

$$k_{str}(\omega)=\frac{\hat{F}_{PWAS}}{\hat{u}_{PWAS}}=\frac{\rho h a^2}{2}\left[\sum_{j_u}\frac{U_{j_u}^2(r_a)}{-\omega^2+2\mathrm{i}\zeta_{j_u}\omega\omega_{ju}+\omega_{j_u}^2}+\left(\frac{h}{2}\right)^2\sum_{j_w}\frac{W_{j_w}'^2(r_a)}{-\omega^2+2\mathrm{i}\zeta_{j_w}\omega\omega_j+\omega_{j_w}^2}\right]^{-1}. \tag{32}$$

Proof. Substitution of the first relation (31) into the last relation (30) gives the modal axial excitation $f_i=\hat{F}_{PWAS}U_j(r_a)$, $j=1,2,\ldots$. Substitution of these expressions into the second equation (30) gives the axial vibration response $u(r,t)=\frac{2}{\rho h a^2}\hat{F}_{PWAS}\sum_{j_u}\frac{U_{j_u}(r_a)}{-\omega^2+2\mathrm{i}\zeta_{j_u}\omega\omega_{j_u}+\omega_{j_u}^2}U_{j_u}(r)\mathrm{e}^{\mathrm{i}\omega t}$ (*). The substitution of the 2nd relation (31) into 2nd relation (24) gives the modal flexural excitation $f_i=-h\hat{F}_{PWAS}W_j'(r_a)/2$, $j=1,2,\ldots$. The substitution of these expressions into the first relation (24) gives finally the flexural vibration response to PWAS excitation $w(r,t)=-\frac{2}{\rho h a^2}\frac{h}{2}\hat{F}_{PWAS}\sum_{j_w}\frac{W_{j_w}'(r_a)}{-\omega^2+2\mathrm{i}\zeta_{j_w}\omega\omega_{j_w}+\omega_{j_w}^2}W_{j_w}(r)\mathrm{e}^{\mathrm{i}\omega t}$ (**). The radial displacement at the edge of the PWAS is of the form $u_{PWAS}(r_a,t)=u(r_a,t)-hw'(r_a,t)$ [9]. Note that $u(r_a,t)$ and $w(r_a,t)$ are the displacements at the plate neutral plan, whereas $u_{PWAS}(r_a,t)$ is measured at the plate upper surface (Fig. 2.2). Discarding the time dependence $\mathrm{e}^{\mathrm{i}\omega t}$, we rewrite this equation in the form $\hat{u}_{PWAS}(r_a)=\hat{u}(r_a)-h\hat{w}'(r_a)/2$. Now, herein substitution of the relations (*), (**) leads to (32).

Now we introduce the concepts and parameters that characterize a circular-shaped PWAS, starting from the piezoelectric constitutive equations in cylindrical coordinates [1, Ch. 7]:

$$S_{rr}=s_{11}^E T_{rr}+s_{12}^E T_{\theta\theta}+d_{31}E_z,\ S_{\theta\theta}=s_{12}^E T_{rr}+s_{11}^E T_{\theta\theta}+d_{31}E_z,\ D_z=d_{31}\left(T_{rr}+T_{\theta\theta}\right)+\varepsilon_{33}^T E_z, \tag{33}$$

where S_{rr} and $S_{\theta\theta}$ are the mechanical strains, T_{rr} and $T_{\theta\theta}$ are the mechanical stresses, E_z is the electrical field, D_z is the electrical displacement, s_{11}^E and s_{12}^E are the mechanical compliances at zero electric field $(E=0)$, ε_{33}^T is the dielectric permittivity at zero mechanical stress $(T=0)$, and d_{31} is the piezoelectric coupling between the electrical and mechanical variables. Hence, $S_{rr}=\partial u_r/\partial r$ and $S_{\theta\theta}=u_r/r$. Applying Newton law of motion, one recovers the wave equation, with a general solution in terms of Bessel function:

$$\frac{\partial^2 u_r}{\partial r^2}+\frac{1}{r}\frac{\partial u_r}{\partial r}-\frac{u_r}{r^2}=\frac{1}{c_p^2}\frac{\partial^2 u_r}{\partial t^2},\ c_P=\sqrt{\frac{1}{\rho s_{11}^E\left(1-v_a^2\right)}},\ u_r(r,t)=AJ_1\left(\frac{\omega r}{c_P}\right)\mathrm{e}^{\mathrm{i}\omega t},\ T_{rr}(r_a)=\frac{k_{\mathrm{str}}(\omega)u_r(r_a)}{t_a}. \tag{34}$$

Last equation (34) expresses the boundary condition. The first two equations (33) give:

$$\begin{aligned}&\left(\partial u_r(r_a)/\partial r\right)=\chi(\omega)(1+\nu_a)u_r(r_a)/r_a-\nu_a u_r(r_a)/r_a+(1+\nu_a)d_{31}E_z,\\&k_{PWAS}=t_a/\left(r_a s_{11}(1-\nu_a)\right),\ \chi(\omega)=k_{str}(\omega)/k_{PWAS},\ \nu_a=-s_{12}^E/s_{11}^E\end{aligned}. \tag{35}$$

The notations refer to, successively: the static stiffness of the circular PWAS, the dynamic stiffness ratio, and the Poisson's ratio of the piezoelectric material. Intermediary, we determine the coefficient A:

$$A=\frac{(1+\nu_a)r_a d_{31}E_z}{\varphi_a J_0(\varphi_a)-(1-\nu_a)+(1+\nu_a)\chi(\omega)J_1(\varphi_a)},\quad \varphi_a=\frac{\omega r_a}{c_P}. \tag{36}$$

The electrical admittance is calculated as the ratio between the current and the voltage amplitudes, i.e., $Y = \hat{I}/\hat{V}$. The current is calculated by integrating the electric displacement D_z over the PWAS area to obtain the total charge, and then differentiating the result with respect to time, whereas the voltage is calculated by multiplying the electric field by the PWAS thickness t_a . Finally the impedance is expressed as:

$$Z(\omega) = \left\{ i\omega C \left[1 - k_p^2 + \frac{k_p^2}{2} \frac{(1+\nu_a) J_0(\varphi_a)}{\varphi_a J_0(\varphi_a) - (1-\nu_a) J_1(\varphi_a) - \chi(\omega)(1+\nu_a) J_1(\varphi_a)} \right] \right\}^{-1}, k_p^2 = \frac{2d_{31}^2}{s_{11}^E (1-\nu_a) \varepsilon_{11}^E}. \quad (37)$$

The complex compliance and dielectric constant expressions can be considered:

$$\bar{\chi}(\omega) = \frac{k_{str}(\omega)}{\bar{k}_{PWAS}}, \bar{k}_{PWAS} = \frac{t_a}{r_a \bar{s}_{11} (1-\nu_a)}, \nu_a = -\frac{s_{12}^E}{s_{11}^E}, \bar{s}_{11} = s_{11}(1-i\eta), \bar{\varepsilon}_{33} = s_{33}(1-i\delta), \bar{C} = C(1-i\mu). \quad (38)$$

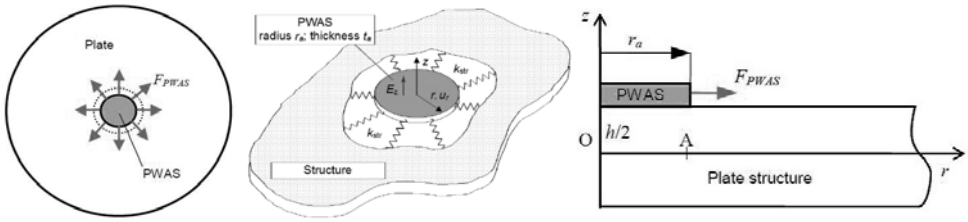

Fig. 2.2 – Circular PWAS constrained by structural stiffness, $k_{str}(\omega)$.

The values of η, δ, μ vary with the piezoceramic formulation of the PWAS material, but are usually small (less than 5%). In this case, we obtain ($\bar{\varphi} = \varphi\sqrt{1-i\eta}$ is also added):

$$Z(\omega) = \left\{ i\omega \bar{C} \left[1 - k_p^2 + \frac{k_p^2}{2} \frac{(1+\nu_a) J_0(\bar{\varphi}_a)}{\bar{\varphi}_a J_0(\bar{\varphi}_a) - (1-\nu_a) J_1(\bar{\varphi}_a) - \chi(\omega)(1+\nu_a) J_1(\bar{\varphi}_a)} \right] \right\}^{-1}, k_p^2 = \frac{2d_{31}^2}{\bar{s}_{11}^E (1-\nu_a) \bar{\varepsilon}_{11}^E} \quad (39)$$

3. EXPERIMENTAL SETUP, NUMERICAL SIMULATION, AND RESULTS

In the experimental setup, the HP 4194A impedance analyzer was used. The chosen geometry for analytical and experimental comparisons is a circular A2024 aluminum plate with a circular Noliac NCE51 PWAS bonded on it (Fig.3.1); the PWAS material is equivalent to the standard PZT-5A material.

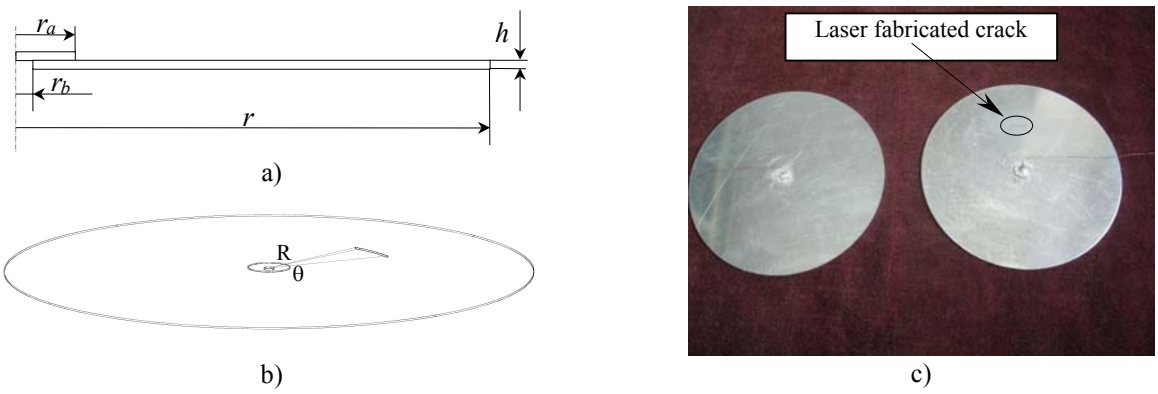

Fig. 3.1 – a) Geometry of the thin plate with central hole and bonded PWAS; b), c) position of the arc-shape crack.

The simulated crack was laser fabricated, in the shape of a circular arc centered on the symmetry center of the plate. Two geometries of the A2024 plates were considered, in FEM simulations, without and with central hole. The central hole was initially used to correctly position the PWAS as centered as possible.

The specimen A2024 with bonded PWAS has the geometry (Fig. 3.1.a,b): r = 50.08mm, h = 0.835mm, r_a = 4mm, r_b = 1mm. The geometry of the simulated crack (0.15mm wide, and 10mm long) is the following (Fig. 3.1a,b): R =25mm, $\theta = 23°$. The adhesive used to bond the PWAS to the A2024 aluminum plate was an electro-conductive epoxy ELPOX15. The thickness of the adhesive layer was measured with a comparator, and was found to be between 20 μm and 100 μm.

The numerical model used in this paper is based on the FEM, and was implemented in the software Comsol 4.3 (Fig. 3.3). A coupled field frequency analysis based on piezoelectric constitutive equations that include structural losses has been taken into consideration, with the following symbol notation:

$$\sigma = \tilde{c}^E \varepsilon - \tilde{e}E,\ D = \tilde{e}\varepsilon + \varepsilon^0 \tilde{\varepsilon}^r E\,, \tag{40}$$

in the stress-charge form; σ is the stress matrix, ε denotes strains matrix, D denotes electric charge matrix, $\tilde{c}^E$ denotes the elasticity matrix, $\tilde{e}$ denotes the piezoelectric coupling matrix, $\tilde{\varepsilon}^r$ the relative permittivity matrix, ~ denotes complex values where the imaginary part defines the dissipative function of the material.

The material of the PWAS was taken PZT5A, that belong to the 6 mm class symmetry, which have compliance, piezoelectric coupling, and relative permittivity matrices in the stress-charge form [11]:

$$\begin{gathered} c_{11}^E = c_{22}^E = 120.35\ \text{GPa}\,,\quad c_{12}^E = 75.18\ \text{GPa}\,,\quad c_{13}^E = c_{23}^E = 75.09\ \text{GPa}\,,\quad c_{33}^E = 110.86\ \text{GPa}\,, \\ c_{44}^E = c_{55}^E = 21.05\ \text{GPa}\,,\quad c_{66}^E = 22.57\ \text{GPa}\,,\quad e_{31} = e_{32} = -5.35116\ \text{C/m}^2\,, \\ e_{33} = 15.7835\ \text{C/m}^2\,,\quad e_{15} = 12.2947\ \text{C/m}^2\,,\quad \varepsilon_{11}^r = \varepsilon_{22}^r = 919.1\,,\quad \varepsilon_{33}^r = 826.6\,. \end{gathered} \tag{41}$$

The mechanical and piezoelectric structural losses for the PWAS were neglected. However the dielectric losses of 1.9% given by the manufacturer were taken into consideration. The mass density of the piezoceramic material was considered $\rho = 7\,750\ \text{kg/m}^3$. The properties of the A2024 aluminum plates were: $E = 73.146\ \text{GPa}$, $\rho = 2\,780\ \text{kg/m}^3$, $\nu = 0.3312$. The adhesive layer being, as shown previously, have a thickness between 20 μm and 100 μm, and transmits most of the shear forces from the PWAS to the thin plate, and therefore was neglected in some cases and considered to be 100 μm in other cases.

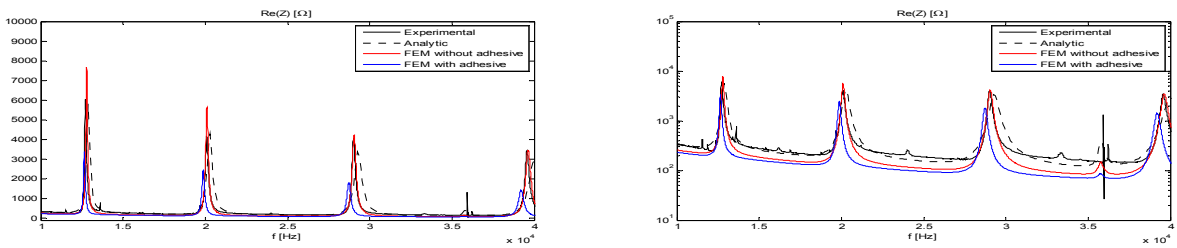

Fig. 3.2 – Real part of the E/M impedance in the case without defect and without central hole:
a) in linear scale; b) in logarithmic scale.

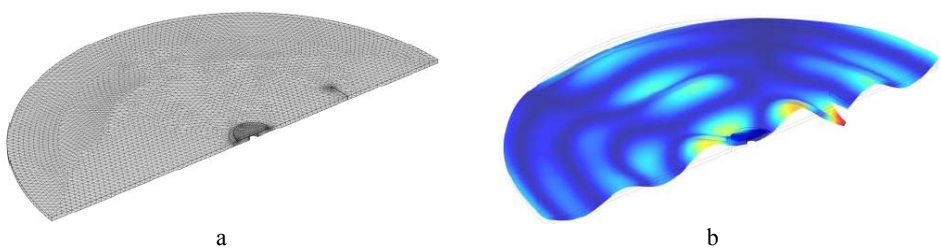

Fig. 3.3 – a) Mesh used in the FEM analysis; b) mode shape of the thin plate with PWAS at 20 kHz, where antiresonance peeks appears, in the case of the defect.

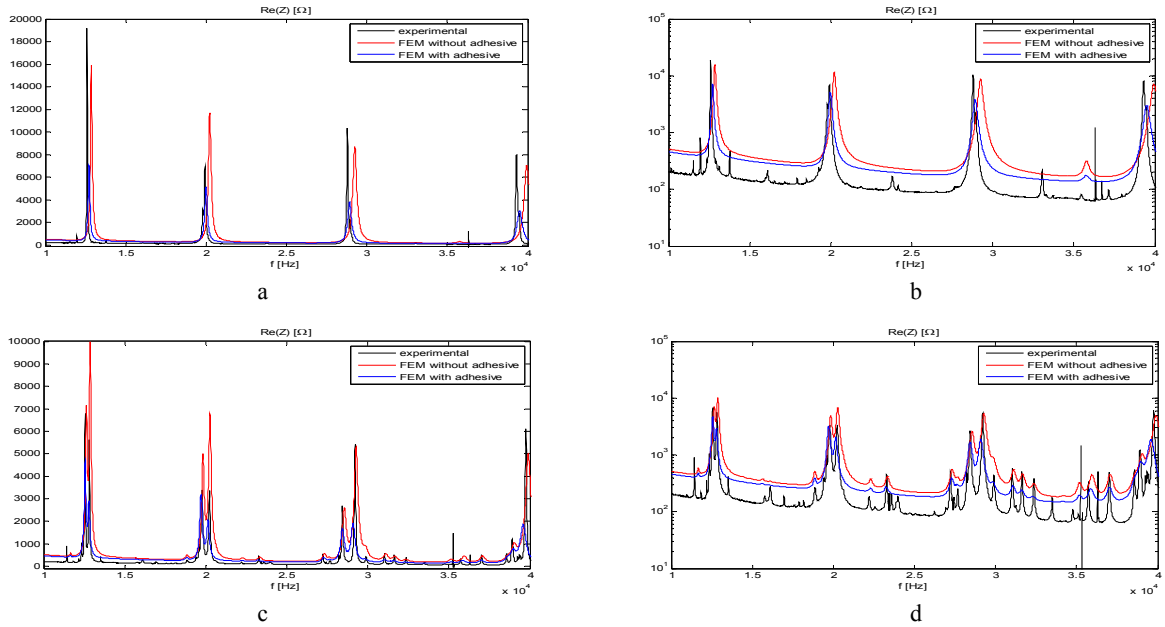

Fig. 3.4 – Re(Z) in the case of thin plate with central hole with bonded PWAS: a), b) without defects, in linear scale (LS), and in logarithmic scale (LogS); c), d) with defect (R = 25mm, θ = 23°), LS and LogS.

Graphics of Re(Z) are presented in Figs. 3.2 and 3.4. It can be seen that the effect of the adhesive layer is not negligible. The FEM analysis shows that there are antiresonance peaks, and the differences are less than 1% in frequency, but larger in amplitude, in the presence of an adhesive layer of 100 μm, compared to the one without adhesive. Because of the axial symmetry, the numerical FEM analysis was done in the 2D axisymmetric mode.

A comparison of the analytic and numerical (FEM) solutions with experiments is done in the frequency range [10kHz, 40kHz] and is given in Fig. 3.2. Analyical solution has input data the geometry and material properties of the A2024 aluminum plate and PWAS. The roots of the characteristic equations (20), (29) are found numerically. The key parameters $\zeta_{j_u} = 0.45\%$ $\zeta_{j_w} = 0.9\%$, $\eta = 2\%$, $\delta = 2\%$ were chosen to match the theoretical results with the experimental data.

Another comparison was made in the case of a plate with central hole, with a laser fabricated crack described above. The presence of central hole is not covered by the theory in this paper, and so the next comparisons were made between experimental data, and FEM analysis with and without adhesive layer. The FEM analyses were done in the 3D mode with XZ symmetry plane; a finer mesh has been taken around the central hole and PWAS, and around the crack (Fig. 3.3.a). Displacements, mode shape of the thin plate with bonded PWAS and with the considered defect at 20 kHz can be seen in Fig. 3.3.b.

It no defect is present, only one antiresonance peek is present. When the defect is present, many antiresonance peeks, appear (Fig. 3.4), visible on the linear scale. From the logarithmic scale, it can be seen that FEM computations follow, also, the smaller peeks that are not easy to observe on the linear scale. It can be seen that an ideal adhesive layer of 100μm, with parallel faces, taken in FEM computations change significantly the shape of the E/M signature. But in real cases, the position of the PWAS is not perfectly parallel to the plate surface, nor perfectly centred, the adhesive layer is not perfect (some delaminations or voids can be present, which can overlap the bonding area etc.), and so significant alteration of the Re(Z) can occur, as it can be seen experimentally and in FEM computations.

4. CONCLUSIONS

The article presents a self-contained study about E/M impedance method for SHM thin circular plates. Comparisons between the analytical method, the finite element method, and experiments were performed, with fabricated structural arc-shape defects. Changes in the E/M impedance spectrum due to presence of a

crack were investigated. It is certified that the E/M impedance method presents the following advantages: small size of the permanently attached or embedded piezoelectric sensors, ultrasonic frequency range application, and ability to be used for on-line and in service SHM.

ACKNOWLEDGEMENTS

The authors gratefully acknowledge the financial support of the National Authority for Scientific Research−ANCS, UEFISCSU, through STAR research project code ID 188/2012.

REFERENCES

1. GIURGIUTIU, V., *Structural Health Monitoring with Piezoelectric Wafer Active Sensors*, Elsevier Academic Press, 2008.
2. ZAGRAI, A., GIURGIUTIU, V., *Electro-mechanical impedance method for crack detection in thin plates,* Journal of Intelligent Material Systems and Structures, **12**, *10*, pp. 709–718, 2001.
3. URSU, I., TECUCEANU, G., TOADER, A., BERAR, V., *Simultaneous active vibration control and health monitoring of structures. Experimental results*, INCAS Bulletin, **2**, *2*, 114–127, 2010.
4. URSU, I., GIURGIUTIU, V., TOADER, A., *Towards spacecraft applications of structural health monitoring*, INCAS Bulletin, **4**, *4*, pp. 111–124, 2012.
5. LEISSA, A., *Vibration of Plates*, NASA SP-160, US Gov't Printing Office, 1969.
6. POISSON, S.-D., *Memoires de l'Academie royale des Sciences de l'Institut de France*, Tome VIII, 1829.
7. ABRAMOWITZ, M., STEGUN, I., *Handbook of Mathematical Functions with Formulas, Graphs, and Mathematical Tables*, Dover Publications, Inc., 1964.
8. ITAO, K., CRANDALL, S. H., *Natural modes and natural frequencies of uniform, circular free-edge plates,* J. Appl. Mech., **46**, 448–453, 1979.
9. KREYSZIG, E., *Advanced Engineering Mathematics*, Wiley, NY, 1968.
10. BICKFORD, W. B., *Advanced Mechanics of Materials*, Addison Wesley Longman, Inc., 1998.
11. *** *Standard on Piezoelectricity,* IEEE std 176-1987; doi: 10.1109/IEEESTD.1988.79638.

Received Decenber 3, 2013